

# Spin-state Crossover Model for the Magnetism of Iron Pnictides

Jiří Chaloupka<sup>1,2</sup> and Giniyat Khaliullin<sup>1</sup>

<sup>1</sup>Max Planck Institute for Solid State Research, Heisenbergstrasse 1, D-70569 Stuttgart, Germany

<sup>2</sup>Central European Institute of Technology, Masaryk University, Kotlářská 2, 61137 Brno, Czech Republic

(Dated: February 9, 2019)

We introduce a minimal model describing magnetic behavior of Fe-based superconductors. The key ingredient of the model is a dynamical mixing of quasi-degenerate spin states of  $\text{Fe}^{2+}$  ion by intersite electron hoppings, resulting in an effective spin  $S_{\text{eff}}$  in the ground state. The moments  $S_{\text{eff}}$  tend to form singlet pairs, and may condense into a spin nematic phase due to the emergent biquadratic exchange couplings. We show that while the spin length  $S_{\text{eff}}$  is robust against the variations of physical parameters, its long-range ordered part may take any value, resolving the puzzle of large but fluctuating Fe-moments observed. Underlying singlet correlations explain also the unusual temperature dependence of the paramagnetic spin susceptibility.

PACS numbers: 75.10.Jm, 74.70.Xa, 71.27.+a

Since the discovery of superconductivity (SC) in  $\text{LaFeAsO}_{1-x}\text{F}_x$  [1], a large number of Fe-based SC's have been found and studied in a great detail [2]. Evidence is mounting that quantum magnetism is an essential part of the physics of Fe-based SC's; in this regard, they are similar to heavy fermion and cuprate SC's. However, the origin of magnetic moments and the mechanisms that suppress their long-range order (LRO) in favor of SC are apparently different from Kondo or Mott physics that operate in rare-earth and cuprate compounds.

The magnetic behavior of Fe-based SC's is unusual. The ordered moments range from  $0.1 - 0.4 \mu_B$ , as in spin-density wave (SDW) metals like Cr, to  $1 - 2 \mu_B$  typical for Mott insulators, causing debates whether the spin-Heisenberg [3–9] or fermionic-SDW pictures [10–14] are more adequate. The external/chemical pressure strongly affects the ordered moment values; however, irrespective to the strength or very presence of LRO, the Fe-ions possess universally the fluctuating moments  $\sim 1 - 2 \mu_B$  [15, 16], even in apparently “nonmagnetic”  $\text{LiFeAs}$  and  $\text{FeSe}$ . In fact, *ab-initio* calculations suggested early on that the Fe-moments, “formed independently on fermiology” [17] and “present all the time” [3], are instrumental to reproduce the measured bond-lengths and phonon spectra [3, 17–19]. Neutron scattering experiments [20] observe intense high-energy spin-waves that are almost independent of doping/temperature, consistent with the picture of local moments induced by Hund's coupling [21] and coexisting with metallic bands.

While the formation of the local moments in orbitally degenerate system is natural, it is surprising that these moments (residing on a simple square lattice) may order or remain disordered, depending on pressure, isovalent substitutions, etc. Moreover, the Fe-pnictides are semimetals where the electron-hole pairs tend to condense into SDW state, further *supporting* magnetic order of the underlying moments. A fragile nature of the magnetic order in Fe-pnictides thus implies the presence of a strong quantum disorder of local moments, not cap-

tured in *ab-initio* calculations that invariably lead to large LRO-moments over an entire phase diagram. The ideas of domain wall motion [18] and local spin fluctuations [21] were proposed as a source of spin disorder, but no clear and tractable model of quantum magnetism in Fe-based SC's has emerged to date. Here we propose such a model.

Since Fe-pnictides are distinct among the other (Mn, Co, Ni-based) pnictide families, their unique physics should be rooted in the specific features of the Fe-ion itself. In fact,  $\text{Fe}^{2+}$  is famous for its spin-crossover [22]: it may adopt either of  $S=0, 1, 2$  states depending on orbital splitting, covalency, and Hund's coupling. As the ionic radius of Fe is sensitive to its spin, Fe- $X$  bond length ( $X$  denotes a ligand) is crucial and pressure reduces the spin value. In oxides,  $S=2$  is typical and  $S=0, 1$  occur at high pressures only (e.g., in the Earth's lower mantle [23]). In compounds with more covalent Fe- $X$  bonds (e.g.,  $X=\text{S}, \text{As}, \text{Se}, \dots$ ),  $S=0$  state is more common while  $S=1, 2$  levels are higher in energy. Here it comes the basic idea of this Letter: when the covalency and Hund's coupling effects compete, the many-body ground state (GS) is a *coherent superposition* of different spin-states intermixed by electron hoppings, resulting in an *average* effective spin  $S_{\text{eff}}$  whose length depends on pressure, doping, etc. We design and solve a model exploring this dynamical spin-crossover idea, and find that: (i) interactions between  $S_{\text{eff}}$  contain large biquadratic exchange and favor singlet pairs, explaining unusual increase of the magnetic susceptibility with temperature [24], (ii) spin-nematic correlations emerge competing with magnetic LRO, (iii) the ordered moments  $m$  vary widely,  $0 \leq m \leq S_{\text{eff}}$ , but magnon spectra are universal and scale with  $S_{\text{eff}}$  as in the experiment [20, 25]. We predict new collective (spin-length fluctuation) modes accessible by resonant x-ray scattering.

The Fe-ions in pnictides have a formal valence state  $\text{Fe}^{2+}(d^6)$ . Among its possible spin states [see Fig. 1(a)],  $S=0$  must have the lowest energy; otherwise, the ordered

moment would be too large and robust. The  $S=0,1$  states, “zoomed-in” further in Fig. 1(b), are most important since they can overlap in the many-body GS by an exchange of just two electrons between two ions, see Fig. 1(c). The corresponding  $\kappa$ -process converts  $\text{Fe}(S=0)\text{-Fe}(S=0)$  pair into  $\text{Fe}(S=1)\text{-Fe}(S=1)$  singlet pair and vice versa; this requires the *interorbital* hopping which is perfectly allowed for  $\sim 109^\circ$  Fe-As-Fe bonding. Basically,  $\kappa$  is a part of usual exchange process when local Hilbert space includes different spin states  $S=0,1$ ; hence  $\kappa \sim J$ . Coupling  $J$  between  $S=1$  triplets is contributed also by their indirect interaction via the electron-hole Stoner continuum. This contribution depends on the Fermi-surface topology and, as the band structure calculations show [26], reduces upon doping since the electron-hole balance of a parent semimetal is no longer perfect.

The Hamiltonian describing the above physics comprises three terms: on-site energy  $E_T$  of  $S=1$  triplet  $T$  relative to  $S=0$  singlet  $s$ , and the bond interactions  $\kappa, J$ :

$$\mathcal{H} = E_T \sum_i n_{T_i} + \sum_{\langle ij \rangle} \left[ -\kappa_{ij} (D_{ij}^\dagger s_i s_j + \text{h.c.}) + J_{ij} \mathbf{S}_i \cdot \mathbf{S}_j \right]. \quad (1)$$

The operator  $D_{ij}^\dagger$  creates a singlet pair of spinfull  $T$ -particles on bond  $\langle ij \rangle$ . For a general spin  $S$  of  $T$ -particles,  $D_{ij} = \sum_M (-1)^{M+S} T_{i,+M} T_{j,-M}$  with  $M = -S, \dots, +S$  denoting the  $N = 2S + 1$  projections; physically,  $N = 3$ . (The normalization factor  $1/\sqrt{N}$  is left out for convenience). The constraint  $n_{s_i} + n_{T_i} = 1$  is implied.

The above model rests on three basic features of Fe-pnictides/chalcogenides: (i) spin-state flexibility of  $\text{Fe}^{2+}$  that can be tuned by pressure increasing  $E_T$ , (ii) edge-sharing  $\text{FeX}_4$  tetrahedral structure allowing “spin-mixing”  $\kappa$ -term, and (iii) semimetallic nature which makes  $J$  values to decrease upon doping [26, 27].

Figure 1(d-f) demonstrates the behavior of the  $N = 3$  model (spin-1  $T$ -particles) on a single bond. The GS wavefunction  $|\psi_{\text{GS}}\rangle = \cos \alpha |\psi_A\rangle + \sin \alpha |\psi_B\rangle$  is a superposition of two singlet states  $|\psi_A\rangle = s_1^\dagger s_2^\dagger |\text{vac}\rangle$  and  $|\psi_B\rangle = \frac{1}{\sqrt{3}} D_{12}^\dagger |\text{vac}\rangle$  mixed by the  $\kappa$ -term. The mixing angle is given by  $\tan 2\alpha = \sqrt{3}\kappa / (E_T - J)$  and the GS energy  $E_{\text{GS}} = E_T - J - \sqrt{(E_T - J)^2 + 3\kappa^2}$ . At  $\kappa = 0$ , there is a sudden jump [Fig. 1(e)] from  $n_T = 0, S = 0$  state to  $n_T = 1, S = 1$  once the exchange energy compensates the cost of having two  $T$ -particles. The dynamical mixing of spin states due to  $\kappa$ -term converts this transition into a spin-crossover: the effective spin length  $S_{\text{eff}} = n_T$  in the GS increases gradually. Fig. 1(f) shows that  $\kappa$ -term strongly stabilizes the singlet pair of  $T$ -particles; we will see that this translates into a large biquadratic coupling  $\propto (\mathbf{S}_1 \cdot \mathbf{S}_2)^2$  which is essential in Fe-pnictides [26, 29].

Turning to the model (1) on a square lattice, we notice first that for  $N \rightarrow \infty$  and large  $\kappa$ , the GS is dominated by tightly bound singlet dimers derived from the single-bond solution. The resonance of dimers on square plaquettes

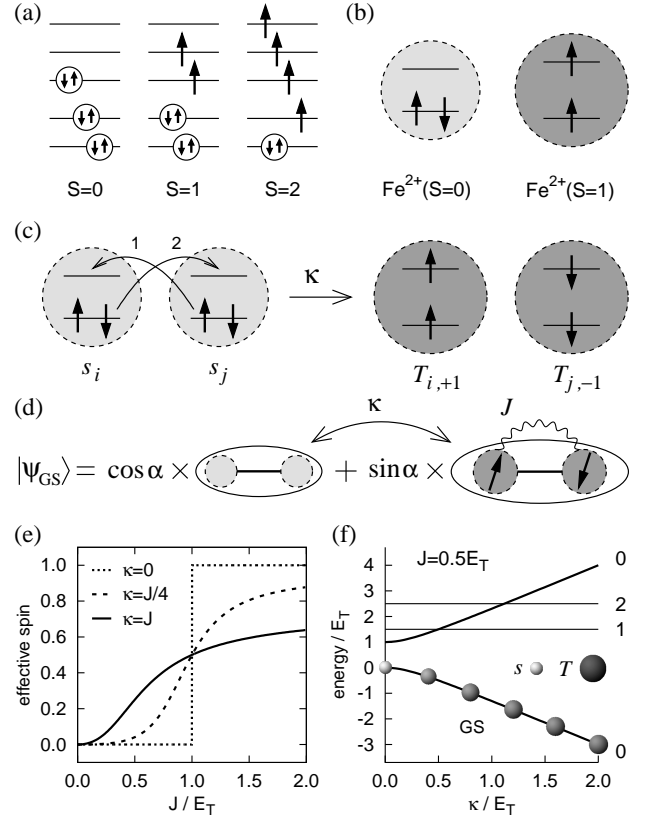


FIG. 1. (a) Schematic view of low ( $S = 0$ ), intermediate ( $S = 1$ ), and high ( $S = 2$ ) spin states of  $\text{Fe}^{2+}(3d^6)$ . (b)  $S = 0$  and  $S = 1$  states differ in two electrons (out of six) occupying either the same or two different  $t_{2g}$  orbitals. (c) The  $\kappa$ -exchange process generating a singlet pair of  $S = 1$  triplets  $T$  of two  $\text{Fe}^{2+}$  ions, both originally in the  $S = 0$  state (denoted by  $s$ ). (d) The GS wavefunction of a  $\text{Fe}^{2+}\text{-Fe}^{2+}$  pair is a coherent superposition of two possible total-singlet states, optimizing energy gain of the  $\kappa$ -processes. (e) Effective spin (average occupation of  $S = 1$  state per Fe-ion), depending on the ratio of the coupling  $J$  between  $S = 1$  states and their energy  $E_T$ . (f) Energy levels labeled by the total spin value of the  $\text{Fe}^{2+}\text{-Fe}^{2+}$  pair. Only singlet pairs are affected by  $\kappa$ . With increasing  $\kappa$ , the  $S = 1$  states are gradually mixed into the GS.

then supports a columnar state [30] breaking lattice symmetry without magnetic LRO. In the opposite limit of  $N = 1$ , the model shows a condensation of hardcore  $T$ -bosons as  $\kappa$  increases (and can be investigated using spin-wave approach [31]). We found that the  $N = 3$  model relevant here is also unstable (at sufficiently large  $\kappa, J$ ) towards a condensation of  $T$ -particles with  $S = 1$ . This condensate hosts interesting correlations not present in a conventional Heisenberg model. We discuss them based on the following variational wavefunction which describes Gutzwiller-projected condensate of spin-1  $T$ -bosons:

$$|\Psi\rangle = \prod_i \left[ \sqrt{1-\rho} s_i^\dagger + \sqrt{\rho} \left( \sum_\alpha d_{\alpha i} T_{\alpha i} \right)^\dagger \right] |\text{vac}\rangle, \quad (2)$$

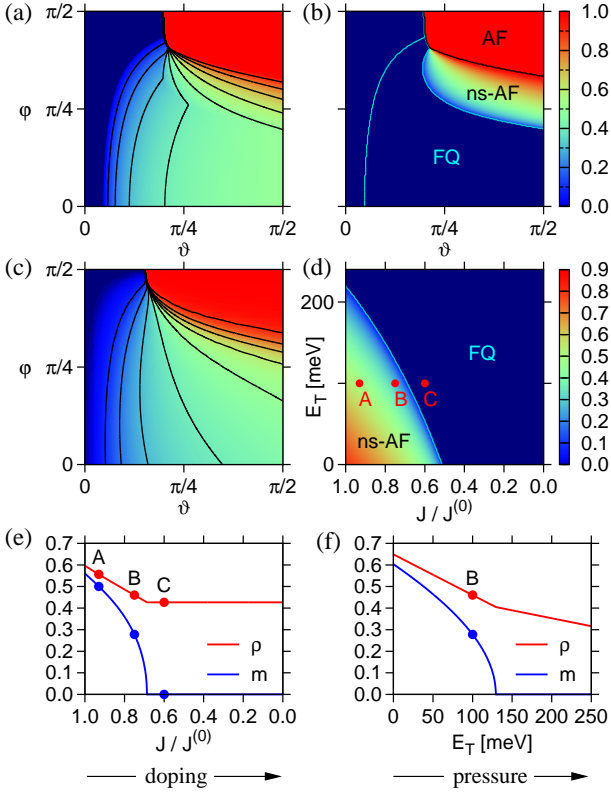


FIG. 2. (color online). (a) Condensate density  $\rho$  ( $\equiv S_{\text{eff}}$ ) obtained from Eq. (2) as a function of angles  $\vartheta, \varphi$  which parametrize the model (1) via  $E_T = \cos \vartheta$ ,  $\kappa_1 = \sin \vartheta \cos \varphi$ , and  $J_1 = \sin \vartheta \sin \varphi$ . We set  $\kappa_2/\kappa_1 = J_2/J_1 = 0.7$ . (b) The ordered spin moment value  $m$ . (c)  $T$ -occupation per site  $n_T$  obtained by an exact diagonalization, to be compared with  $\rho$  of panel (a). A bipartite 12-site cluster defined by the vectors  $(2, 2)$  and  $(-4, 2)$  in the square lattice was used. (d) Phase diagram and the ordered moment  $m$  as a function of  $E_T$  and relative  $J$ -strength for fixed  $\kappa_1 = 100$  meV,  $\kappa_2 = 0.7\kappa_1$ ,  $J_1^{(0)} = 140$  meV,  $J_2^{(0)} = 0.7J_1^{(0)}$ . (e,f) Effective spin-length  $\rho = S_{\text{eff}}$  and ordered moment  $m$  at the (e)  $E_T = 100$  meV and (f)  $J/J^{(0)} = 0.75$  lines through the phase diagram in (d).

where  $\rho \in [0, 1]$  is the condensate density to be understood as the effective spin length  $S_{\text{eff}}$ . The complex unit vectors  $\mathbf{d}_i = \mathbf{u}_i + i\mathbf{v}_i$  ( $u_i^2 + v_i^2 = 1$ ) determine the spin structure of the condensate in terms of the coherent states of spin-1 [32, 33] corresponding to the operators  $T_\alpha$  ( $\alpha = x, y, z$ ):  $T_x = (T_{+1} - T_{-1})/\sqrt{2}i$ ,  $T_y = (T_{+1} + T_{-1})/\sqrt{2}$ ,  $T_z = iT_0$ . This is advantageous due to the symmetric expressions  $D_{ij} = \sum_\alpha T_{i\alpha}T_{j\alpha}$  and  $S^\alpha = -i\epsilon_{\alpha\beta\gamma}T_\beta^\dagger T_\gamma$ . The GS phase diagram obtained by minimizing  $\langle \Psi | \mathcal{H} | \Psi \rangle$  and cross-checked by an exact diagonalization on a small cluster is presented in Fig. 2. We have included nearest-neighbor (NN) and next-NN interactions and fixed their ratio at  $J_2/J_1 = \kappa_2/\kappa_1 = 0.7$ , reflecting large next-NN overlap via As ions. Like in  $J_1 - J_2$  model, this ratio decides between  $(\pi, \pi)$  and  $(\pi, 0)$  order. Fig. 2(a,b) contains, apart from a disordered (un-

condensed) phase ( $\rho = 0$ ) at small  $\kappa, J$ , three distinct phases depending on  $\kappa/E_T$  and  $J/E_T$  values: (i) Ferroquadrupolar (FQ) phase with  $\mathbf{u}_i = \mathbf{u}$  of unit length and zero  $\mathbf{v}_i$ . This phase is characterized by the quadrupolar order parameter  $\langle S^\alpha S^\beta - \frac{1}{3}S^2\delta_{\alpha\beta} \rangle = \rho(\frac{1}{3}\delta_{\alpha\beta} - u_\alpha u_\beta)$  with  $\mathbf{u}$  playing the role of the quadrupolar *director* [33], but it has zero magnetization. This state, often referred to as *spin-nematic*, appears in biquadratic-exchange [32–35] and spin-1 optical lattice models [36–39]. (ii) Nonsaturated antiferromagnetic (ns-AF) phase with stripy magnetic order, specified by  $\mathbf{u}_i = (0, 0, u)$  and  $\mathbf{v}_i = (0, v, 0)e^{i\mathbf{Q}\cdot\mathbf{R}_i}$  with  $\mathbf{Q} = (\pi, 0)$ . The LRO-moment is given by  $m = 2\rho uv$  which can take values from 0 to  $S_{\text{eff}} = \rho$ , even on a classical level. (iii) Saturated antiferromagnet (AF) with the same  $\mathbf{Q}$  vector, but now with  $u = v = 1/\sqrt{2}$  and the ordered spin moment  $m = S_{\text{eff}} = 1$ .

The part of the phase diagram relevant to pnictides is shown in Fig. 2(d). The decrease of  $J$  is associated with doping that changes the nesting conditions [26], while the increase of  $E_T$  is related to external/chemical pressure. Fig. 2(e,f) shows that the LRO-moment  $m$  quickly vanishes as  $J$  ( $E_T$ ) values decrease (increase); however, the spin-length  $S_{\text{eff}} = \rho$  remains almost constant ( $\sim 1/2$ ), corresponding to a fluctuating magnetic moment  $\sim 1\mu_B$ . This quantum state is driven by  $\kappa$ -process which generates the spin-1 states in a form of singlet pairs.

We consider now the excitation spectrum, focusing on a realistic case of large condensate density ( $\rho \gtrsim 0.4$ ). It is convenient to separate fast (density) and slow (spin) fluctuations. To this end we introduce pseudospin  $\tau = 1/2$  indicating the presence of a  $T$ -particle, and a normalized vector field  $\mathbf{d}$  defining the spin-1 operator as  $\mathbf{S} = -i(\mathbf{d}^\dagger \times \mathbf{d})$  [classical part of  $\mathbf{d}$  enters Eq. (2)]. The Hamiltonian then reads as

$$\mathcal{H} = E_T \sum_i \left( \frac{1}{2} - \tau_i^z \right) - \sum_{\langle ij \rangle} \kappa_{ij} (\tau_i^+ \tau_j^+ \mathbf{d}_i \cdot \mathbf{d}_j + \text{h.c.}) - \sum_{\langle ij \rangle} J_{ij} \left( \frac{1}{2} - \tau_i^z \right) \left( \frac{1}{2} - \tau_j^z \right) (\mathbf{d}_i^\dagger \times \mathbf{d}_i) \cdot (\mathbf{d}_j^\dagger \times \mathbf{d}_j), \quad (3)$$

and is decoupled on a mean-field level. The condensate spin dynamics is given by  $O(3)$ -symmetric Hamiltonian

$$\mathcal{H}_d = - \sum_{\langle ij \rangle} \tilde{\kappa}_{ij} (\mathbf{d}_i \cdot \mathbf{d}_j + \text{h.c.}) - \sum_{\langle ij \rangle} \tilde{J}_{ij} (\mathbf{d}_i^\dagger \times \mathbf{d}_i) \cdot (\mathbf{d}_j^\dagger \times \mathbf{d}_j) \quad (4)$$

with the renormalized  $\tilde{\kappa}_{ij} = \kappa_{ij} \langle \tau_i^+ \tau_j^+ \rangle \approx \kappa_{ij}(1 - \rho)\rho$  and  $\tilde{J}_{ij} \approx J_{ij}\rho^2$ . The excitations above the GS (2) are found by introducing  $a, b, c$  bosons according to  $\mathbf{d} = (d_x, d_y, d_z) = (a, ub - iv e^{i\mathbf{Q}\cdot\mathbf{R}} c, -iv e^{i\mathbf{Q}\cdot\mathbf{R}} b + uc)$ , and replacing the condensed one as  $c, c^\dagger \rightarrow \sqrt{1 - n_a - n_b}$ . The resulting quadratic part of the  $a, b$  Hamiltonian is solved by the Bogoliubov transformation. A similar approach is used for the  $\tau$ -sector Hamiltonian describing the condensate density fluctuations  $\delta\rho$ .

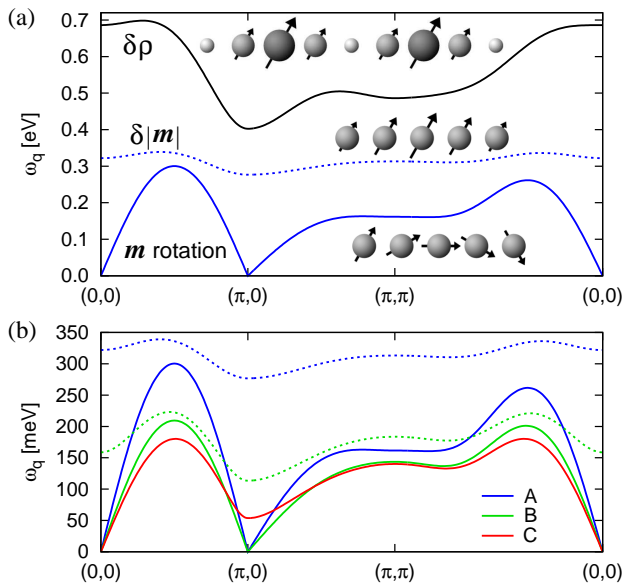


FIG. 3. (color online). (a) Dispersion of the condensate density ( $\delta\rho$ , solid-black) and the ordered moment-length ( $\delta|m|$ , dotted-blue) fluctuations, and the magnon dispersion (solid-blue), at the point *A* in the phase diagram of Fig. 2(d). All 3 modes are active with respect to resonant x-ray scattering, and the latter 2 to neutron scattering. (b) Evolution of the magnetic excitations going from FQ to the ns-AF phase [*C*  $\rightarrow$  *B*  $\rightarrow$  *A* in Fig. 2(d)]. Two-fold degenerate quadrupole-waves (*C*) split into the magnon (solid lines) and the  $\delta|m|$  mode (dotted lines). The latter represents oscillations between the nematic and magnetic orderings and is gapful.

Shown in Fig. 3 is the dispersion of the excitations for several points of the phase diagram. The density (i.e.,  $S_{\text{eff}}$ ) fluctuations are high in energy. Fig. 3(b) focuses on the magnetic excitations. In the FQ phase, quadrupole/magnetic modes are degenerate and gapless at  $\mathbf{q} = 0$ , where they correspond to the Goldstone modes associated with a free director rotation. As the ns-AF phase is approached, the gap at  $\mathbf{Q}$  decreases, and closes upon entering the magnetic phase. Importantly, the spin fluctuation spectra is determined by the effective spin  $S_{\text{eff}} = \rho$  and not by the ordered moment  $m$  value. Since  $\rho$  varies only slightly, the magnon energies should be common to different materials, as in fact observed [20, 25].

The magnetic modes in Fig. 3(b) resemble excitations of bilinear-biquadratic spin model [33]. In fact, the dispersion in FQ phase can be *exactly* reproduced [40] from an effective spin-1 model  $\sum_{\langle ij \rangle} \tilde{J}_{ij} \mathbf{S}_i \cdot \mathbf{S}_j - \tilde{\kappa}_{ij} (\mathbf{S}_i \cdot \mathbf{S}_j)^2$ , with  $\tilde{J}$  and  $\tilde{\kappa}$  shown above. A large biquadratic coupling was indeed found to account for many observations in iron pnictides [8, 26, 29]. We note however, that this model possesses FQ and AF phases only and misses the ns-AF phase, where the ordered moment is reduced already at the classical level; also, it does not contain the key notion of the original spin-crossover model, i.e., formation of the effective spin  $S_{\text{eff}}$  and its fluctuations.

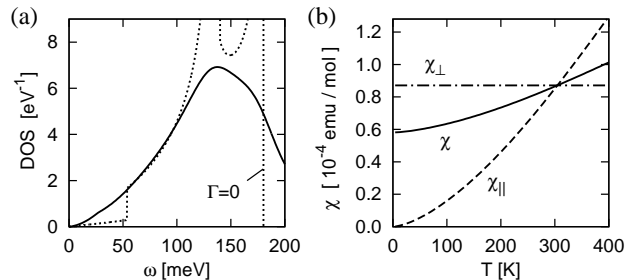


FIG. 4. (a) Density of states of the magnetic excitations calculated for the point *C* of Fig. 2(d). We included the damping (e.g., due to coupling to the Stoner continuum) in a form  $\Gamma(\omega) = \min(\omega, \Gamma)$  with  $\Gamma = \omega\mathbf{Q}/2$ . The result with  $\Gamma = 0$  is shown for comparison. (b) Temperature dependence of the uniform susceptibility  $\chi$ . The components  $\chi_{\parallel}$  ( $\chi_{\perp}$ ) parallel (perpendicular) to the local director  $\mathbf{u}$  are also shown. Low-energy cutoff of 1 meV was used.

Singlet correlations inherent to the model may explain also unusual increase of the paramagnetic susceptibility  $\chi(T)$  with temperature [24]. Considering non-magnetic FQ phase, we find that for the field parallel to the director  $\mathbf{u}$ ,  $\chi$  is temperature dependent,  $\chi_{\parallel} = \frac{1}{2T} \int d\omega \mathcal{N}(\omega) \sinh^{-2} \frac{\omega}{2T}$ , where  $\mathcal{N}(\omega) = \sum_{\mathbf{q}} \delta(\omega - \omega_{\mathbf{q}})$  is the density of states (DOS) of magnetic excitations, while  $\chi_{\perp}$  for the field perpendicular to  $\mathbf{u}$  is constant and inversely proportional to the bandwidth of excitations. (The physical  $\chi$  contains additional factor of  $\rho^2 g^2 \mu_B^2 N_A$  with  $g = 2$  and the Avogadro number  $N_A$ ). Their average  $\chi = (\chi_{\parallel} + 2\chi_{\perp})/3$  with respect to the local director orientation corresponds to the measured  $\chi(T)$ , assuming slow rotations of the director. The DOS shown in Fig. 4(a) is contributed mainly by the regions around  $(\pi, 0)$  and  $(0, \pi)$  where AF correlations do reside. The corresponding thermal excitations lead to the increase of  $\chi$  up to very high temperatures [see Fig. 4(b)].

To conclude, we proposed the model describing quantum magnetism of Fe-pnictides. Their universal magnetic spectra, wide-range variations of the LRO-moments, emergent biquadratic-spin couplings are explained. The model stands also on its own: extending the Heisenberg models to the case of “mixed-spin” ions, it represents novel many-body problem explored here only in part and deserves future study. Of a particular interest is the effect of band fermions (only mentioned above as the origin of doping dependent  $J$  values and magnon damping) which should have a strong impact on low energy dynamics of the model, e.g., converting the  $\mathbf{q} = 0$  Goldstone modes into overdamped spin-nematic fluctuations. Understanding the effects of coupling between local moments and band fermions, including implications for SC, should be the next step towards a complete theory of Fe-pnictides.

We thank G. Jackeli for useful discussions. JC acknowledges support by the Alexander von Humboldt Foundation, ERDF under project CEITEC

(CZ.1.05/1.1.00/02.0068) and EC 7<sup>th</sup> Framework Programme (286154/SYLICA).

- 
- [1] Y. Kamihara *et al.*, J. Am. Chem. Soc. **130**, 3296 (2008).  
 [2] For a review of the experimental data, see, e.g., D.C. Johnston, Adv. Phys. **59**, 803 (2010).  
 [3] T. Yildirim, Physica C **469**, 425 (2009).  
 [4] C. Xu, M. Müller, and S. Sachdev, Phys. Rev. B **78**, 020501(R) (2008).  
 [5] Q. Si and E. Abrahams, Phys. Rev. Lett. **101**, 076401 (2008).  
 [6] C. Fang *et al.*, Phys. Rev. B **77**, 224509 (2008).  
 [7] G. Uhrig *et al.*, Phys. Rev. B **79**, 092416 (2009).  
 [8] D. Stanek, O.P. Sushkov, and G. Uhrig, Phys. Rev. B **84**, 064505 (2011).  
 [9] R. Yu *et al.*, arXiv:1112.4785.  
 [10] I.I. Mazin, D.J. Singh, M.D. Johannes, and M.H. Du, Phys. Rev. Lett. **101**, 057003 (2008).  
 [11] K. Kuroki *et al.*, Phys. Rev. Lett. **101**, 087004 (2008).  
 [12] A.V. Chubukov, D.V. Efremov, and I. Eremin, Phys. Rev. B **78**, 134512 (2008).  
 [13] S. Graser, T.A. Maier, P.J. Hirschfeld, and D.J. Scalapino, New J. Phys. **11**, 025016 (2009).  
 [14] E. Kaneshita, T. Morinari, and T. Tohyama, Phys. Rev. Lett. **103**, 247202 (2009).  
 [15] H. Gretarsson *et al.*, Phys. Rev. B **84**, 100509(R) (2011).  
 [16] P. Vilmercati *et al.*, Phys. Rev. B **85**, 220503(R) (2012).  
 [17] M.D. Johannes, I.I. Mazin, and D.S. Parker, Phys. Rev. B **82**, 024527 (2010).  
 [18] I.I. Mazin and M.D. Johannes, Nature Phys. **5**, 141 (2009).  
 [19] D. Reznik *et al.*, Phys. Rev. B **80**, 214534 (2009).  
 [20] M. Liu *et al.*, Nature Phys. **8**, 376 (2012).  
 [21] Z.P. Yin, K. Haule, and G. Kotliar, Nature Mater. **10**, 932 (2011).  
 [22] P. Gütlich and H.A. Goodwin (Eds.), *Spin Crossover in Transition Metal Compounds I* (Springer, Berlin, 2004).  
 [23] S. Stackhouse, Nature Geosci. **1**, 648 (2008).  
 [24] R. Klingeler *et al.*, Phys. Rev. B **81**, 024506 (2010).  
 [25] J.T. Park *et al.*, Phys. Rev. B **86**, 024437 (2012).  
 [26] A.N. Yaresko, G.-Q. Liu, V.N. Antonov, and O.K. Andersen, Phys. Rev. B **79**, 144421 (2009).  
 [27] Orbital degeneracy of  $S = 1$  triplets (relevant for electronic nematicity [28] and tetra/ortho transition) can be readily included in the model.  
 [28] S. Kasahara *et al.*, Nature **486**, 382 (2012).  
 [29] A.L. Wysocki, K.D. Belashchenko, and V.P. Antropov, Nature Phys. **7**, 485 (2011).  
 [30] N. Read and S. Sachdev, Phys. Rev. Lett. **62**, 1694 (1989).  
 [31] K. Bernardet *et al.*, Phys. Rev. B **65**, 104519 (2002).  
 [32] B.A. Ivanov and A.K. Kolezhuk, Phys. Rev. B **68**, 052401 (2003).  
 [33] A. Läuchli, F. Mila, and K. Penc, Phys. Rev. Lett. **97**, 087205 (2006).  
 [34] H. Tsunetsugu and M. Arikawa, J. Phys. Soc. Jpn. **75**, 083701 (2006).  
 [35] K. Harada and N. Kawashima, Phys. Rev. B **65**, 052403 (2002).  
 [36] E. Demler and F. Zhou, Phys. Rev. Lett. **88**, 163001 (2002); A. Imambekov, M. Lukin, and E. Demler, Phys. Rev. B **68**, 063602 (2003).  
 [37] S.K. Yip, Phys. Rev. Lett. **90**, 250402 (2003).  
 [38] C.M. Puetter, M.J. Lawler, and H.-Y. Kee, Phys. Rev. B **78**, 165121 (2008).  
 [39] M. Serbyn, T. Senthil, and P.A. Lee, Phys. Rev. B **84**, 180403(R) (2011).  
 [40] This can be understood using the identity  $(\mathbf{S}_i \cdot \mathbf{S}_j)^2 = |\mathbf{d}_i \cdot \mathbf{d}_j|^2 + 1$ . If  $v \ll u \approx 1$ , like in the FQ phase or close to it in the ns-AF phase, we recover the  $\kappa$ -term of Eq. (4):  $(\mathbf{S}_i \cdot \mathbf{S}_j)^2 \approx \mathbf{d}_i \cdot \mathbf{d}_j + \mathbf{d}_i^\dagger \cdot \mathbf{d}_j^\dagger$ .